

Supporting Information for ”On the intermittency of orographic gravity wave hotspots and its importance for middle atmosphere dynamics”

A. Kuchar¹, P. Sacha^{2,3}, R. Eichinger^{4,5}, Ch. Jacobi¹, P. Pisoft¹, Harald E.

Rieder³

¹Institute for Meteorology, Universität Leipzig, Stephanstr. 3, 04103 Leipzig, Germany

²Department of Atmospheric Physics, Faculty of Mathematics and Physics, Charles University, V Holesovickach 2, 180 00 Prague 8,

Czech Republic

³Institute of Meteorology and Climatology, University of Natural Resources and Life Sciences, Vienna (BOKU),

Gregor-Mendel-Strasse 33, 1180 Vienna, Austria

⁴Meteorological Institute, Ludwig-Maximilians-University (LMU), Munich, Germany

⁵Deutsches Zentrum für Luft- und Raumfahrt (DLR), Institut für Physik der Atmosphäre, Oberpfaffenhofen, Germany

Contents of this file

1. Figures S1 to S13

Introduction

For understanding the middle-atmospheric circulation, a useful quantitative framework based on transformed Eulerian-mean (TEM) equations has been developed and is still abundantly used despite its limitations (Haynes, 2005), e.g. small-amplitude wave disturbances and zonally symmetric basic flows. The transformation leading to the TEM

equations was introduced by D. Andrews and McIntyre (1978, 1976); Boyd (1976). Using TEM equations in spherical (φ), log-pressure¹ coordinates, we document how in the two-dimensional perspective wave forcing affects the mean flow (\bar{u}) as well as the meridional transport:

$$\bar{u}_t + \bar{v}^* \left[(\rho_0 a \cos \varphi)^{-1} (\bar{u} \cos \varphi)_\varphi - f \right] + \bar{w}^* \bar{u}_z = (\rho_0 a \cos \varphi)^{-1} \nabla \cdot \vec{F} + R \equiv \mathcal{F} \quad (\text{S1})$$

where f is the Coriolis parameter², a is the earth's radius, ρ_0 is a standard reference density and R denotes the residual term representing sub-grid scale processes such as GWD and numerical diffusion. The vector \vec{F} is known as the Eliassen-Palm (EP) flux:

$$F^{(\varphi)} = \rho_0 a \cos \varphi \left(\bar{u}_z \overline{v' \theta'} / \bar{\theta}_z - \overline{v' u'} \right), \quad (\text{S2})$$

$$F^{(z)} = \rho_0 a \cos \varphi \left\{ \left[f - (\rho_0 a \cos \varphi)^{-1} (\bar{u} \cos \varphi)_\varphi \right] \overline{v' \theta'} / \bar{\theta}_z - \overline{w' u'} \right\} \quad (\text{S3})$$

together used in the EP flux divergence (EPFD):

$$\nabla \cdot \vec{F} = (a \cos \varphi)^{-1} \left(F^{(\varphi)} \cos \varphi \right)_\varphi + F_z^{(z)} \quad (\text{S4})$$

Overbars and primes denote zonal mean and anomalies from the zonal mean, respectively.

The subscripts denote derivatives.

References

- Andrews, D., & McIntyre, M. (1978). Generalized Eliassen-Palm and Charney-Drazin theorems for waves on axisymmetric mean flows in compressible atmospheres. *Journal of the Atmospheric Sciences*, 35(2), 175–185.
- Andrews, D., & McIntyre, M. E. (1976). Planetary waves in horizontal and vertical shear: The generalized Eliassen-Palm relation and the mean zonal acceleration. *Journal of the Atmospheric Sciences*, 33(11), 2031–2048.

- Andrews, D. G., & McIntyre, M. E. (1987). *JR Holton, and CB Leovy, 1987: Middle Atmosphere Dynamics*. Academic Press.
- Boyd, J. P. (1976). The noninteraction of waves with the zonally averaged flow on a spherical earth and the interrelationships on eddy fluxes of energy, heat and momentum. *Journal of the Atmospheric Sciences*, 33(12), 2285–2291.
- Haynes, P. (2005). Stratospheric Dynamics. *Annual Review of Fluid Mechanics*, 37(1), 263–293. Retrieved from <http://www.annualreviews.org/doi/abs/10.1146/annurev.fluid.37.061903.175710> doi: 10.1146/annurev.fluid.37.061903.175710

Notes

1. $z = -H \ln(p/p_s)$ where p_s is a standard reference pressure (usually $\approx 10^3$ hPa) and H is a mean scale height (usually ≈ 7 km) (D. G. Andrews & McIntyre, 1987).
2. It equals to $2\Omega \sin \varphi$ where $\Omega \doteq 7.292 \cdot 10^{-5} \text{ s}^{-1}$ is the earth's rotation rate.

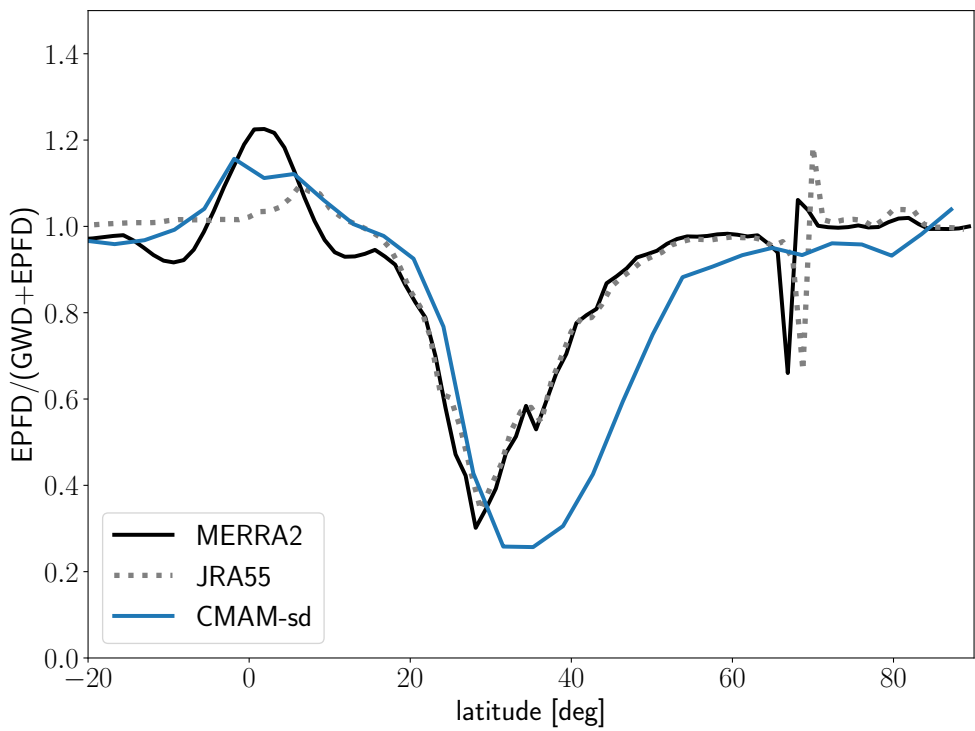


Figure 1. Climatological relative EPFD contribution to the overall drag (EPFD+total GWD) in January averaged over the period 1980-2010. Black dotted line represents JRA55. Black solid line represents MERRA2 and blue solid line represents CMAM-sd.

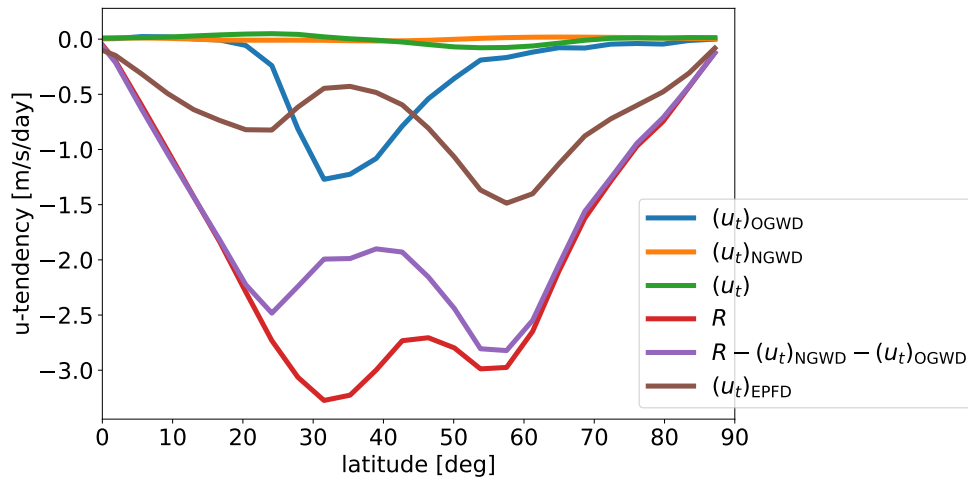


Figure S2. Climatological average of particular CMAM-sd tendencies in January averaged over the period 1980-2010. R was calculated from eq. S1 as a difference between $(\rho_0 a \cos \varphi)^{-1} \nabla \cdot \vec{F}$ labeled as $(u_t)_{\text{EPFD}}$ and the left side of the equation. $(u_t)_{\text{OGWD}}$ or $(u_t)_{\text{NGWD}}$ origins from outputs of CMAM30 parameterizations, respectively.

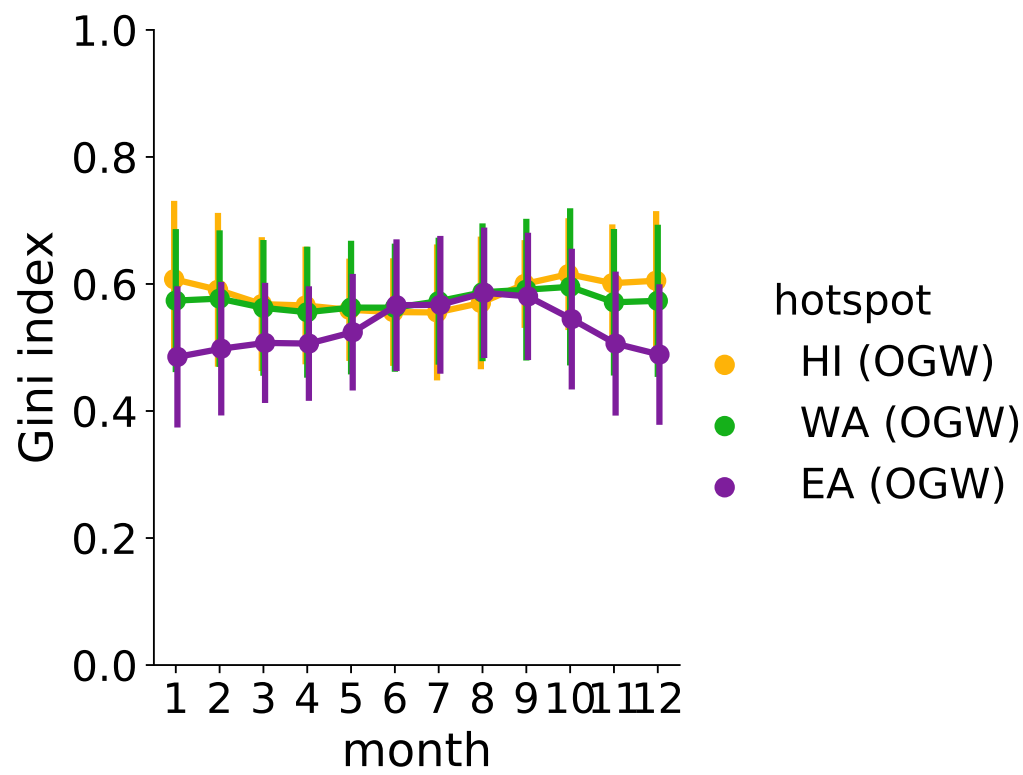


Figure S3. Spatial and annual variability of Gini index of OGW momentum fluxes at 850 hPa within Himalayas, East Asia and West America hotspot, respectively. Error bars show spatial standard deviation.

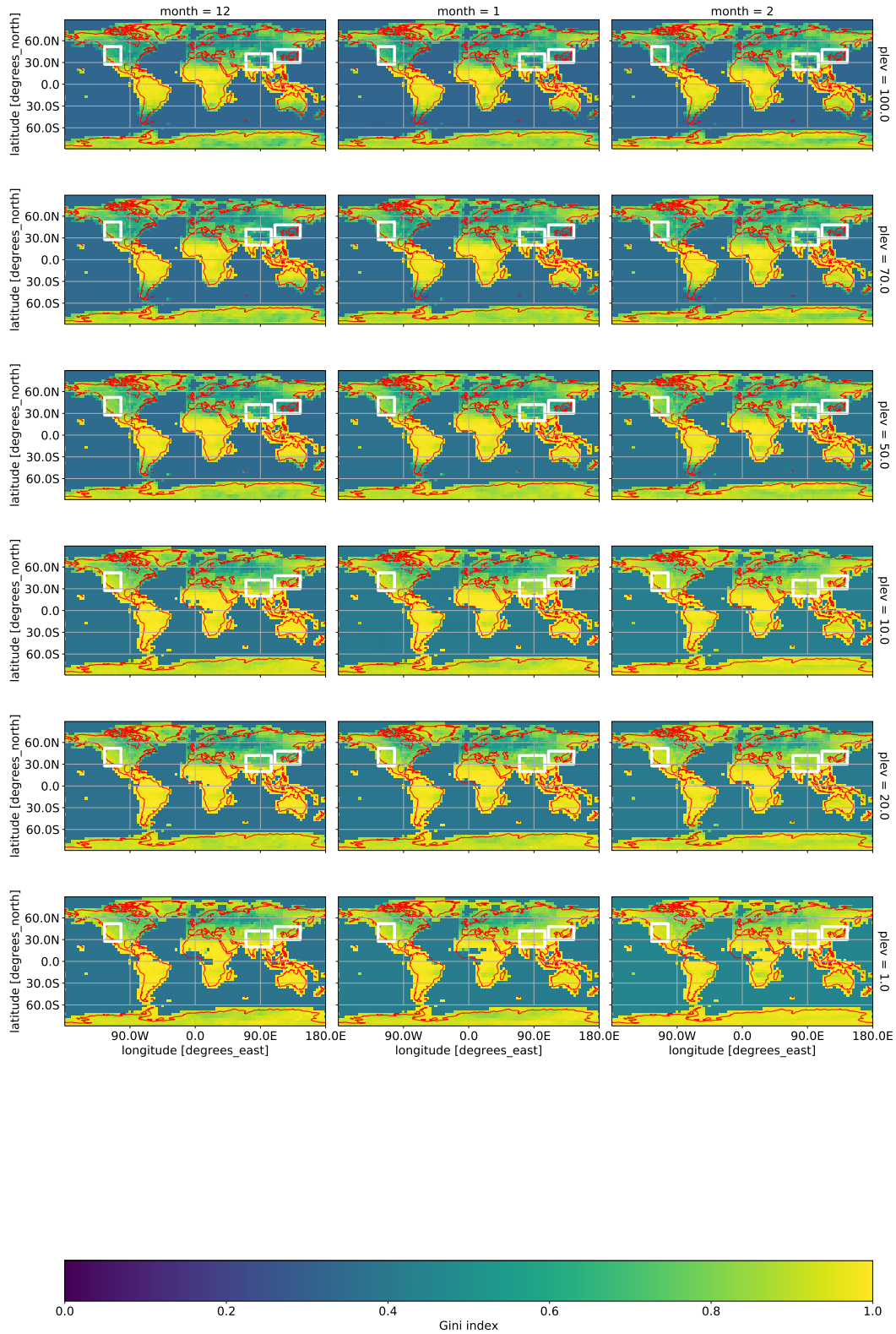


Figure S4. Spatial variability of Gini index of OGW momentum fluxes at {100, 70, 50, 20, 10, 1} hPa for December, January and February, respectively.

May 2, 2020, 9:58am

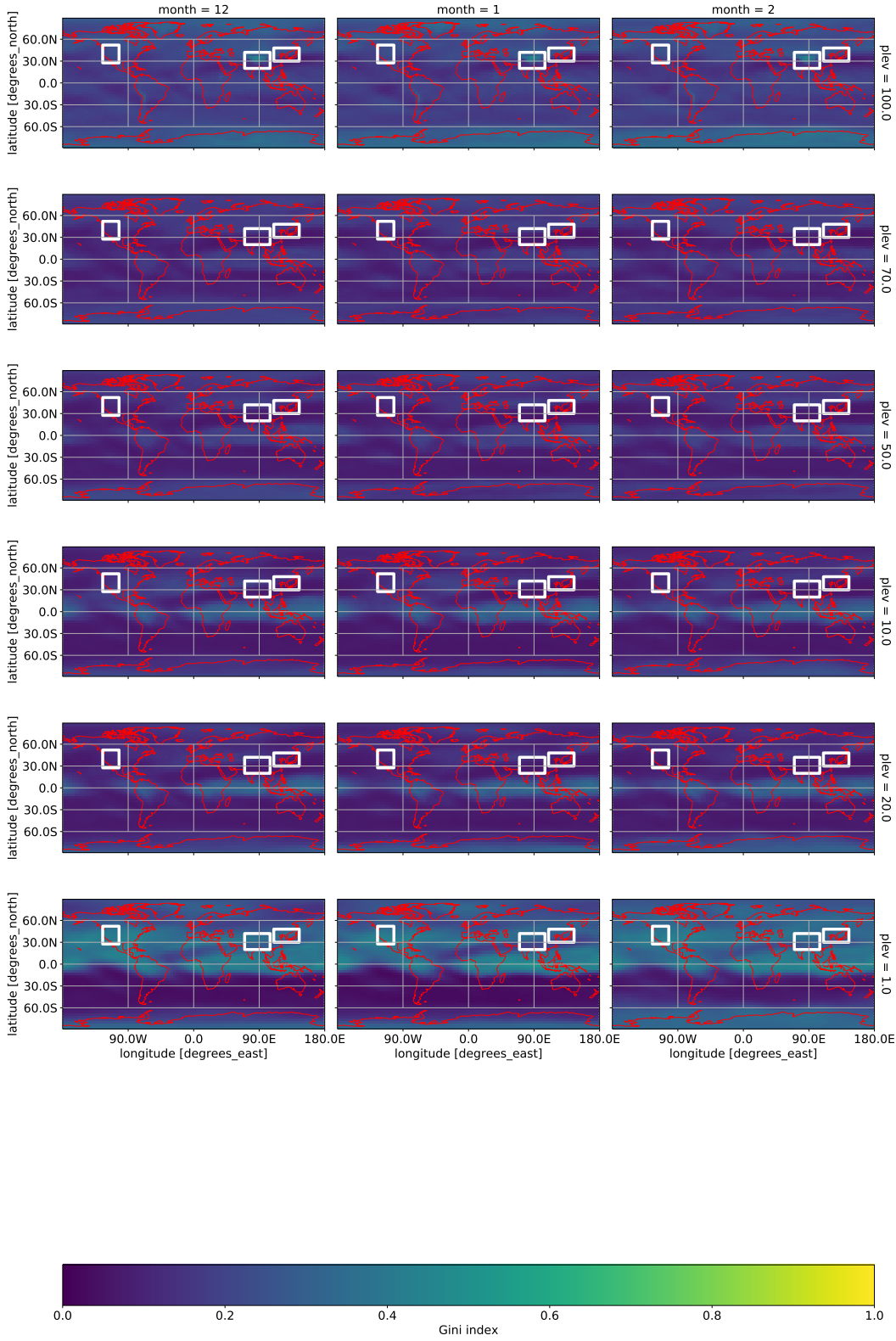


Figure S5. Spatial variability of Gini index of NOGW momentum fluxes at $\{100, 70, 50, 20, 10, 1\}$ hPa for December, January and February, respectively.

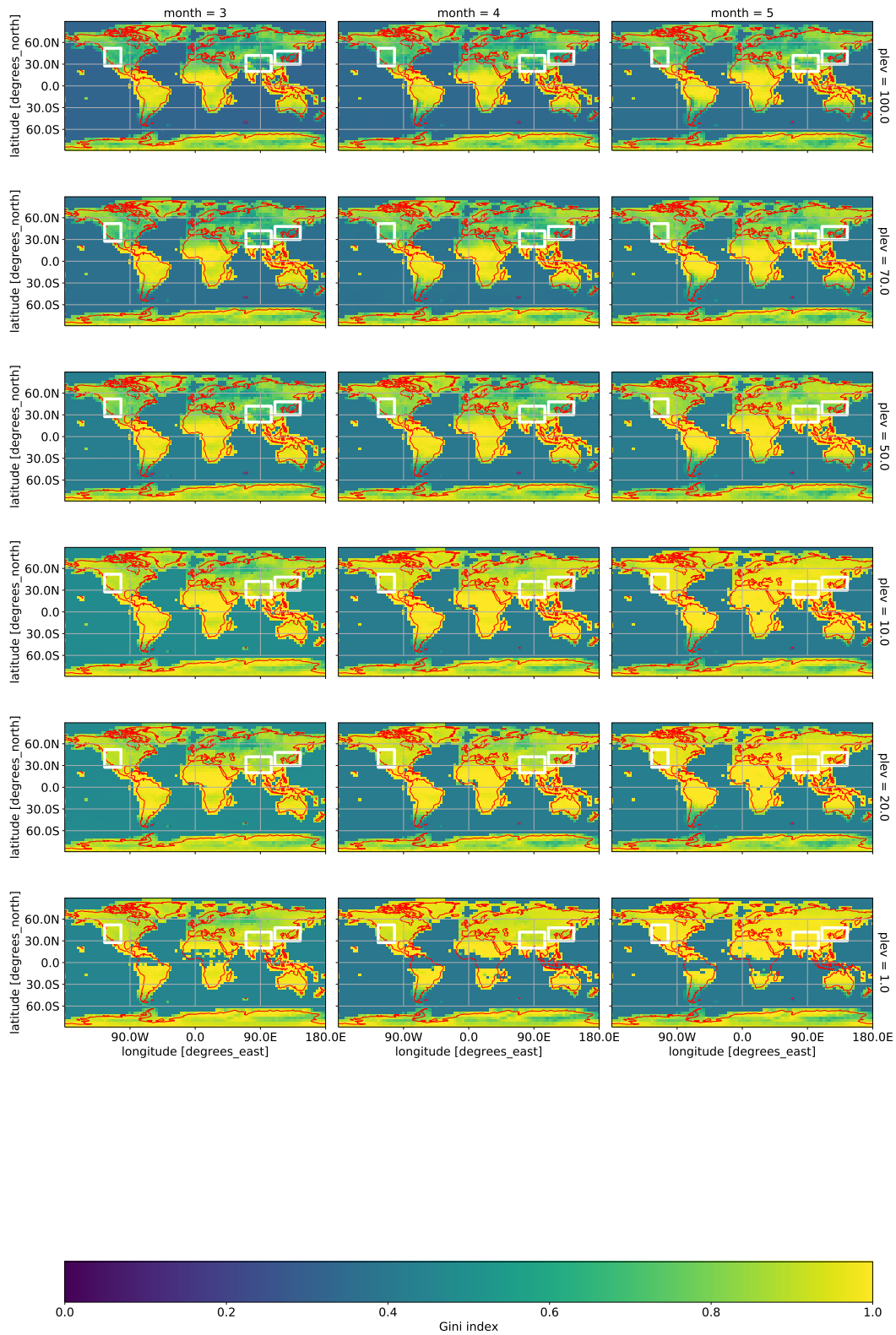


Figure S6. Spatial variability of Gini index of OGW momentum fluxes at $\{100, 70, 50, 20, 10, 1\}$ hPa for March, April and May, respectively.

May 2, 2020, 9:58am

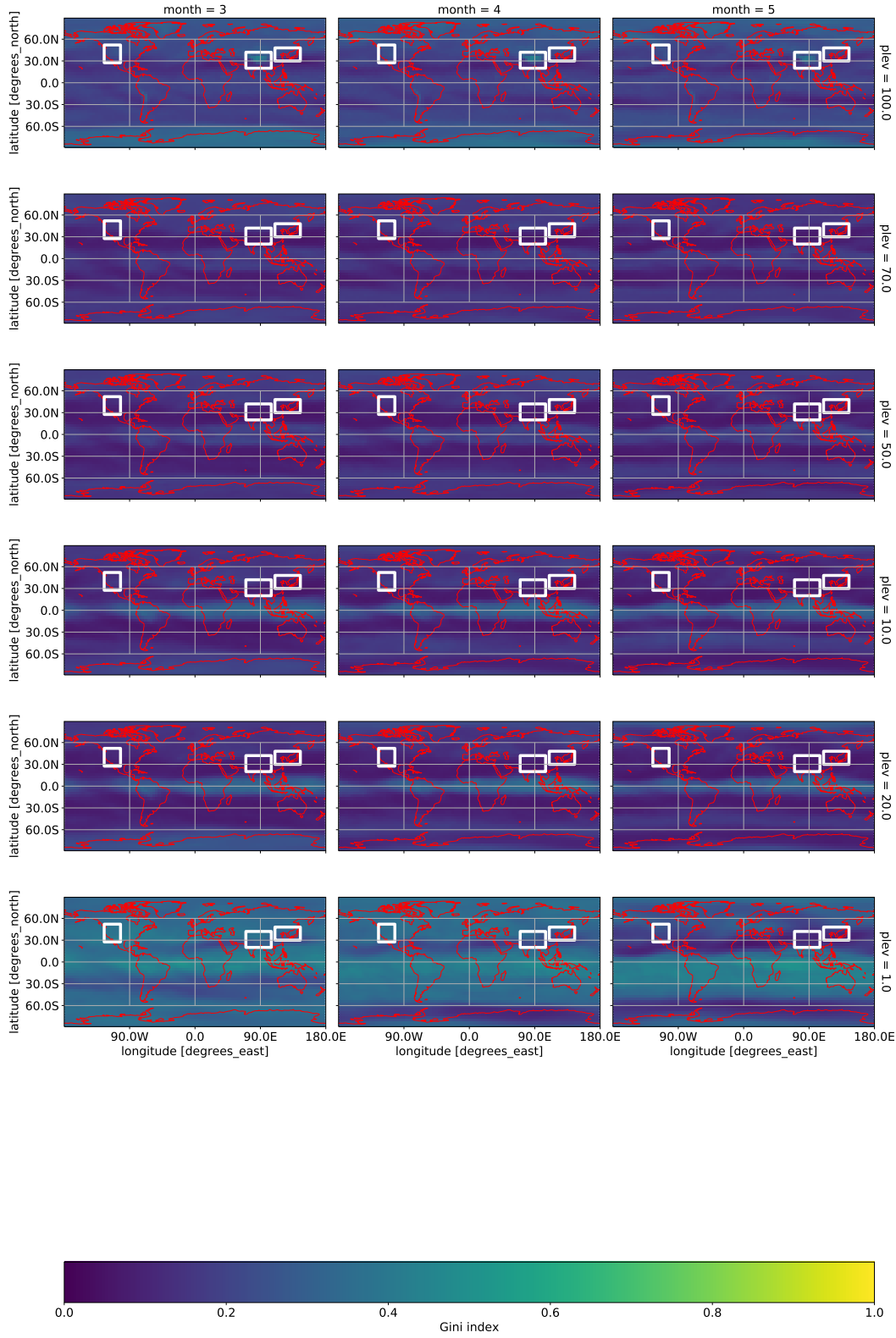


Figure S7. Spatial variability of Gini index of NOGW momentum fluxes at $\{100, 70, 50, 20, 10, 1\}$ hPa for March, April and May, respectively.

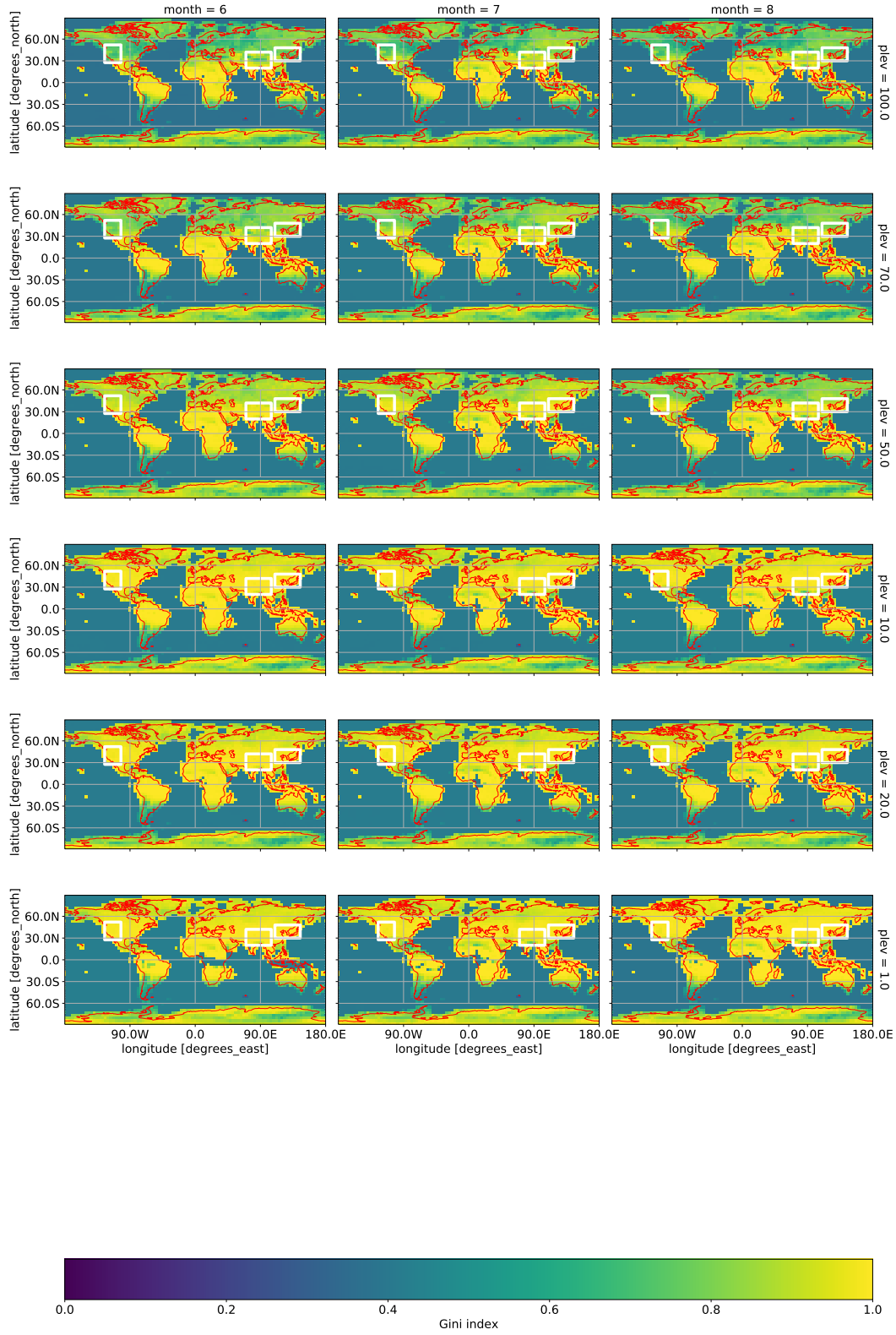


Figure S8. Spatial variability of Gini index of OGW momentum fluxes at {100, 70, 50, 20, 10, 1} hPa for June, July and August, respectively.

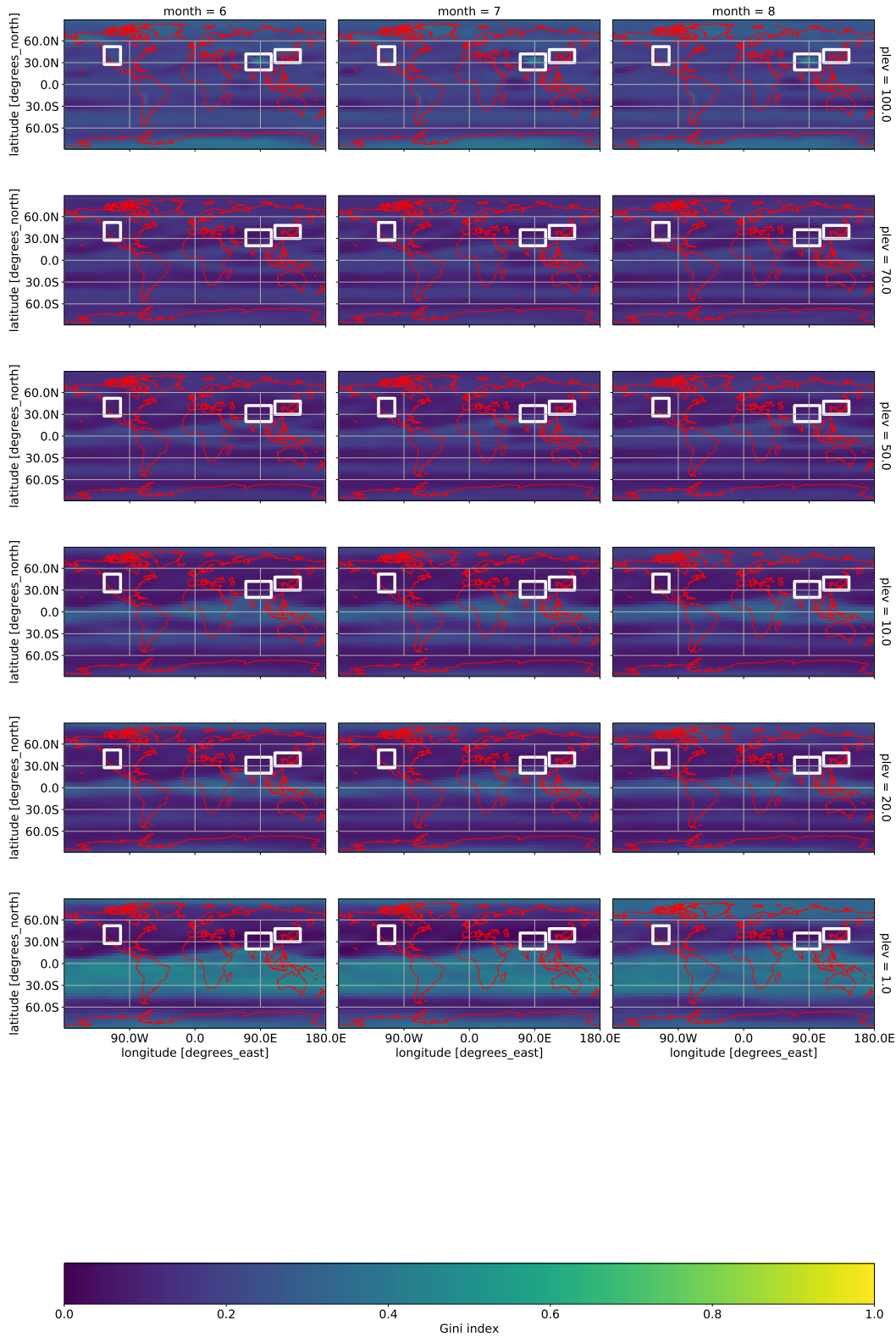


Figure S9. Spatial variability of Gini index of NOGW momentum fluxes at $\{100, 70, 50, 20, 10, 1\}$ hPa for June, July and August, respectively.

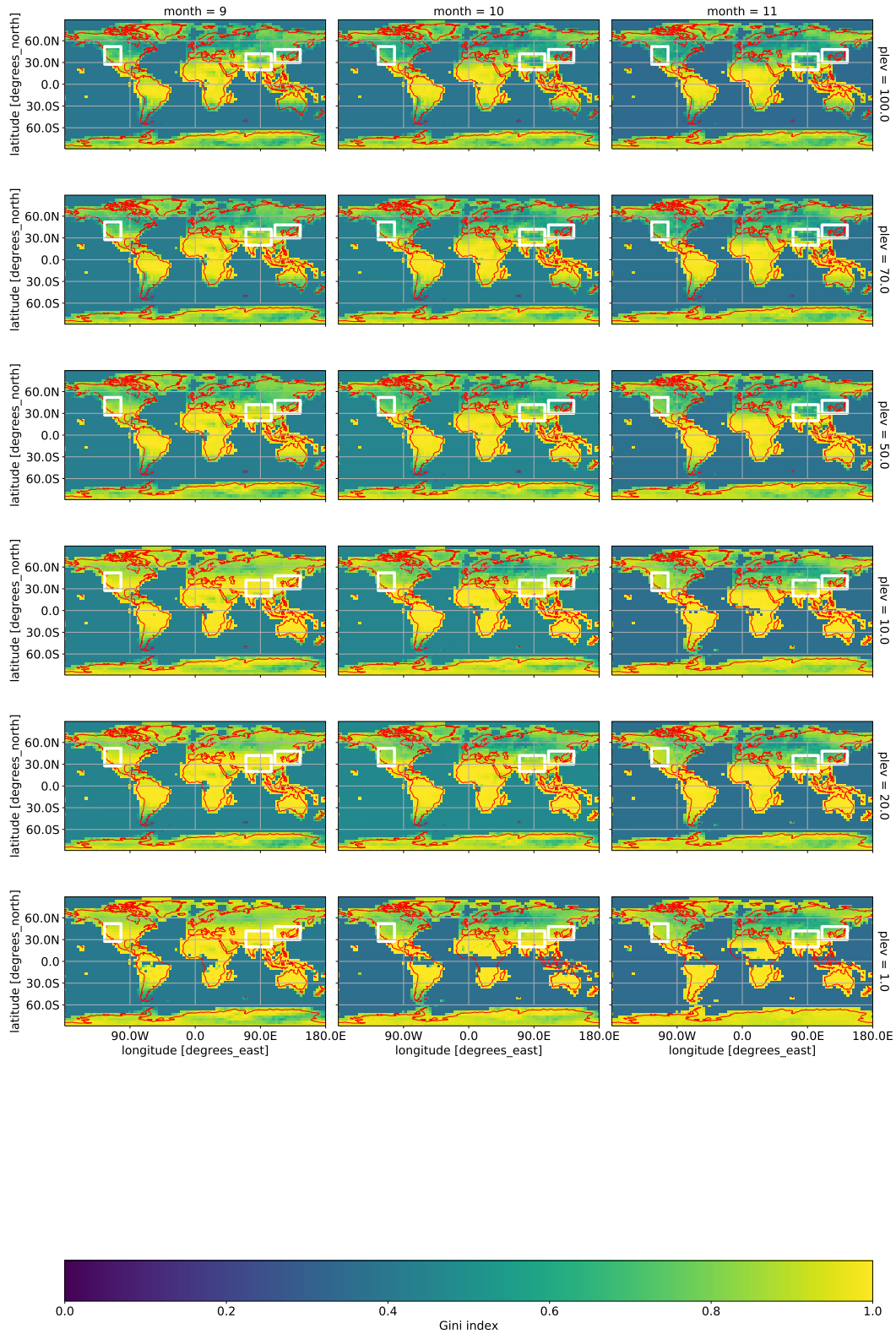


Figure S10. Spatial variability of Gini index of OGW momentum fluxes at $\{100, 70, 50, 20, 10, 1\}$ hPa for September, October and November, respectively.

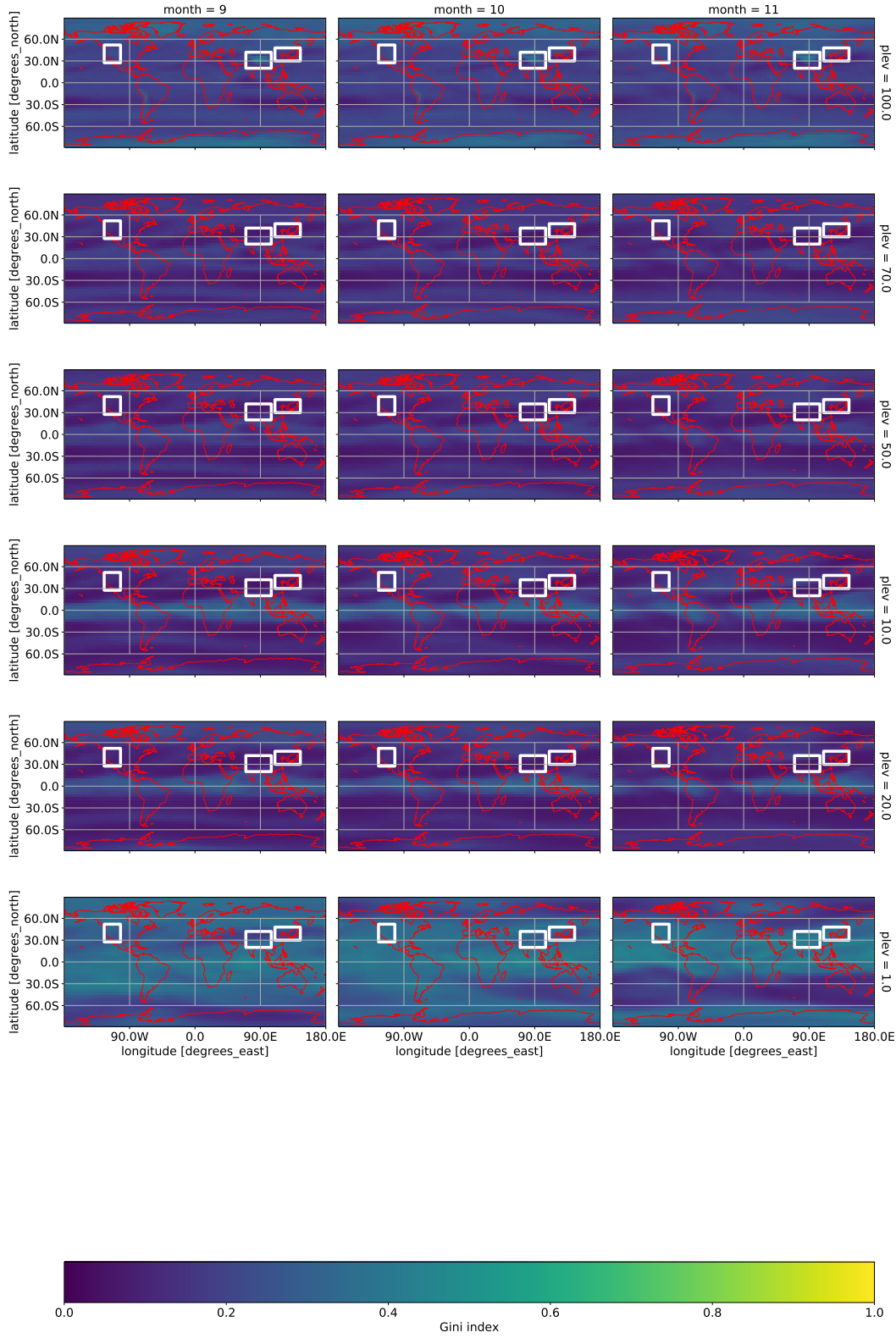


Figure S11. Spatial variability of Gini index of NOGW momentum fluxes at $\{100, 70, 50, 20, 10, 1\}$ hPa in September, October and November, respectively.

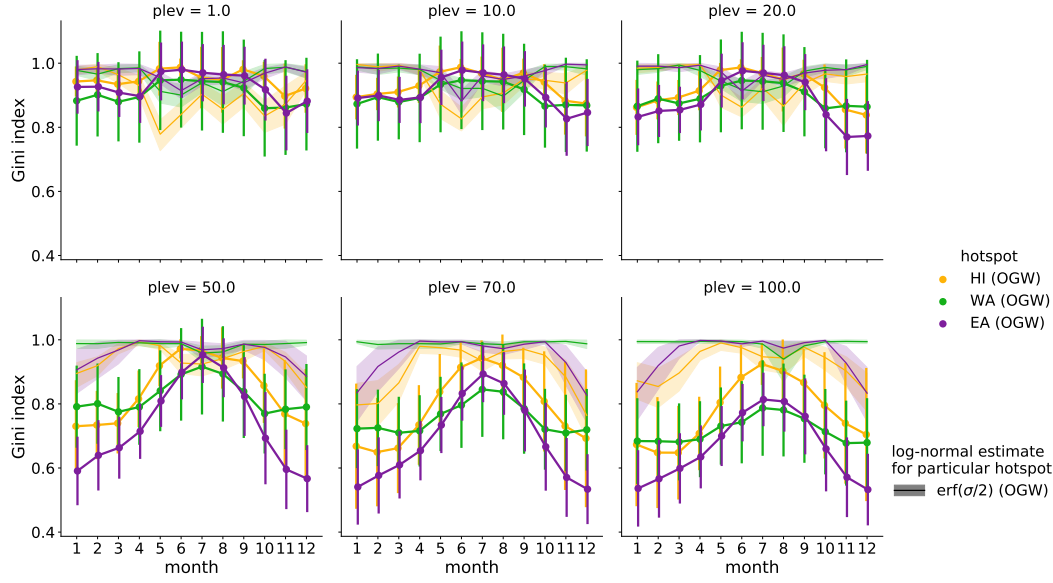


Figure S12. Spatial and annual variability of the Gini coefficient of OGW momentum fluxes at 100, 70, 50, 20, 10, 1 hPa within the Himalaya, East Asia and West America hotspot, respectively. Solid lines with circles and error bars represent the calculated Gini coefficient. Lines with error bands denote the Gini coefficient from the log-normal distribution estimate according to Eq. 2 in the main text. Error bars show the spatial standard deviation.

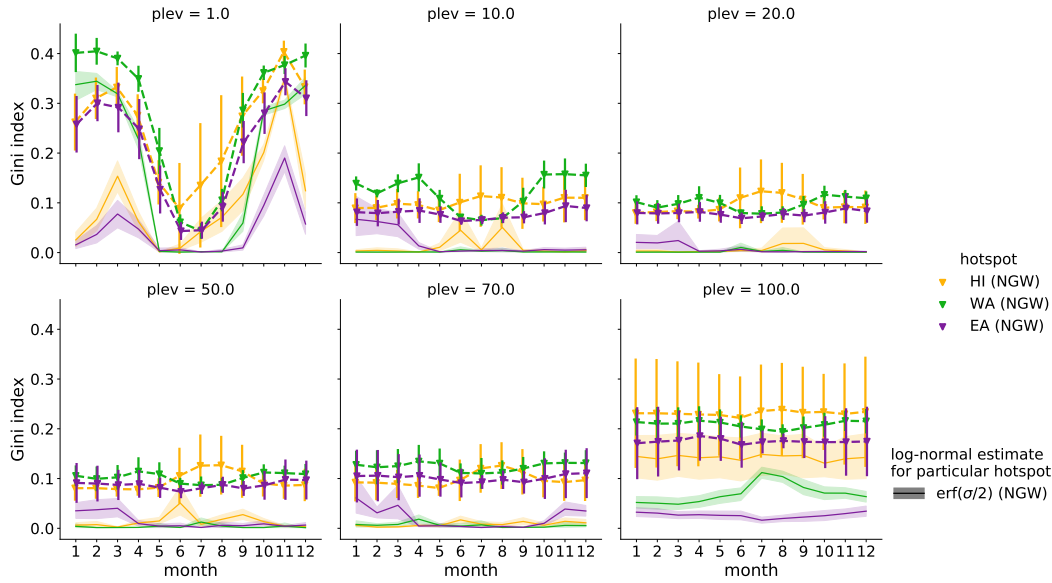


Figure S13. Spatial and annual variability of the Gini coefficient of NOGW momentum fluxes at 100, 70, 50, 20, 10, 1 hPa within the Himalaya, East Asia and West America hotspot, respectively. Dashed lines with triangles and error bars represent the calculated Gini coefficient. Lines with error bands denote the Gini coefficient from the log-normal distribution estimate according to Eq. 2 in the main text. Error bars show the spatial standard deviation.